

From superconducting fluctuations to the bosonic limit in the response functions above the critical temperature

G.C. Strinati and P. Pieri

Dipartimento di Matematica e Fisica, Sezione INFM

Università di Camerino, I-62032 Camerino, Italy

(December 2, 2024)

We investigate the density, current, and spin response functions *above* the critical temperature for a system of three-dimensional fermions interacting via an attractive short-range potential. In the strong-coupling (bosonic) limit of this interaction, we identify the dominant diagrammatic contributions for a “dilute” system of composite bosons which form as bound-fermion pairs, and compare them with the usual (Aslamazov-Larkin, Maki-Thompson, and density-of-states) terms occurring in the theory of superconducting fluctuations above the critical temperature for a clean system in the weak-coupling limit. We show that, at the zeroth order in the diluteness parameter for the composite bosons, the Aslamazov-Larkin term still represents formally the dominant contribution to the density and current response functions, while the Maki-Thompson and density-of-states terms are strongly suppressed. Corrections to the Aslamazov-Larkin term are then considered at the next order in the diluteness parameter for the composite bosons. The spin response function is also examined, and it is found to be exponentially suppressed in the bosonic limit only when appropriate sets of diagrams are considered simultaneously.

PACS numbers: 74.40, 74.20.-z, 05.30.Jp

I. INTRODUCTION

Response functions constitute an essential tool for connecting experimentally measurable quantities with the theoretical description of a condensed-matter system. Specifically, knowledge of density, current, spin, and heat response functions allows one to test the relevance of the degrees of freedom which are selected in an approximate description of a complex system.

In particular, for superconductors the current response function plays a special role since the Meissner effect can be demonstrated by examining its behavior.¹ Within the standard BCS (weak-coupling) theory, the transverse current response function below the critical temperature can be readily evaluated by representing it as a particle-hole bubble in terms of normal and anomalous single-particle propagators,^{1,2} while above the critical temperature the standard expression for a noninteracting Fermi gas is obtained, with no sign of superconductivity being evidenced in this way when approaching the transition from above. (For the longitudinal current response function below the critical temperature, corrections to the particle-hole bubble need instead to be included in order to maintain gauge invariance.¹)

In the weak-coupling limit, precursor effects of superconductivity *above* the critical temperature have been considered (especially for reduced dimensionality), by introducing *pairing fluctuations* in the Fermi gas due to the same attractive interaction which is responsible for the formation of the superconducting state below the critical temperature. In this way, the so-called Aslamazov-Larkin (AL),³ Maki-Thompson (MT),⁴ as well as the density-of-state (DOS) contributions have been evaluated

and tested against experimental data, for superconducting samples of reduced dimensionality⁵ and for strongly anisotropic cuprate superconductors in the overdoped region.⁶ No corresponding analysis has, however, been performed in the strong-coupling limit, where composite bosons form due to the strong fermionic attraction.

Concerning the cuprate superconductors, the small value of the (superconducting) coherence length and the presence of a pseudogap above the critical temperature in the underdoped region^{7,8} (which could be related to pairing) have suggested the possible relevance of a *crossover* scenario from a weak-coupling limit for overdoped samples (with Cooper pairs forming and condensing at the critical temperature within a BCS description) toward a strong-coupling limit for underdoped samples, whereby preformed (composite) bosons would exist above the superconducting critical temperature and Bose-Einstein condense below it.^{9–13} (For cuprate superconductors, it seems likely that the pairing is actually in an *intermediate* regime between overlapping Cooper pairs and non-overlapping composite bosons.)

In this context, it appears relevant to study how the response functions evolve between the two (weak- and strong-) coupling limits, by examining specifically how the response of the original Fermi system can be interpreted in terms of the response of an effective Bose system in the strong-coupling limit. This evolution of the response functions rests on the fact that the fluctuation propagator, which constitutes the building block of fluctuation theory in the weak-coupling limit *above* the superconducting critical temperature, acquires the form of the propagator for composite bosons in the strong-coupling limit. Akin to the selection of the fermionic

self-energy diagrams already considered,¹⁴ we select the dominant (diagrammatic) contributions to the response functions in the strong-coupling (bosonic) limit by relying on the “diluteness” condition of the system. This procedure, which is *a priori* complementary to the selection of fluctuation diagrams usually considered in the weak-coupling limit, will result into the *same* diagrams for the response functions as far as the dominant interaction contribution (over and above the noninteracting-fermion contribution) is concerned. The finding that the same diagrams constitute the dominant interaction contribution to the response functions *both* in the weak- and strong-coupling limit provides us with an interpolation scheme which could be used to explore the interesting intermediate-coupling regime where no classification of diagrams can be relied on. By this token, one can follow the evolution of the response functions from weak to strong coupling (or vice versa), in a similar fashion to what has been already done for ground-state properties¹⁵ and for finite-temperature thermodynamic quantities¹⁶.

The systematic procedure for selecting the contributions to the response functions which are dominant *in the strong-coupling limit* rests, on the one hand, on certain integrals (that contain products of fermionic single-particle Green’s functions) acquiring a particularly simple form in the strong-coupling limit, and, on the other hand, on the standard classification of bosonic diagrams in the “dilute” limit.¹⁷ In this way, the contributions to the response functions are organized in powers of the diluteness parameter as well as of the (inverse of the) fermionic chemical potential. It is, in fact, the property of the fermionic chemical potential to constitute the largest energy scale in the strong-coupling limit which considerably simplifies dealing with this limit.

We shall consider a Fermi system with an attractive (point-contact) interparticle interaction, embedded in a three-dimensional continuum and *above* the superconducting critical temperature. No lattice or impurities effects will be taken into account. Consideration of the broken-symmetry case below the critical temperature is postponed to future work. The two-dimensional case, where superconducting fluctuations are enhanced, will also be considered separately owing to peculiar problems arising in this case for the crossover from weak to strong coupling.

Besides providing a detailed analysis of the current response function, in this paper we shall also examine the density and spin response functions and determine how they evolve from weak to strong coupling. In this context, we will show that the spin response function requires certain diagrammatic contributions to be included simultaneously, in order for this response function to vanish correctly in the strong-coupling limit when fermions pair into spin-zero composite bosons.

The plan of the paper is as follows. Section II discusses the current response function at the leading and next-to-leading order in the “diluteness” parameter for composite bosons. In Section III the density and spin

response functions are considered. Section IV gives our conclusions.

II. CURRENT RESPONSE FUNCTION

In this Section, we identify the leading diagrammatic contributions to the current response function for a system of fermions with an attractive interparticle interaction in the strong-coupling limit. These contributions are then carried over to the weak-coupling limit, to which the standard theory of superconducting fluctuations above the critical temperature applies.

Knowledge of the detailed form of the fermionic attractive interaction V_{eff} is not required for studying the evolution from the weak- to strong-coupling limit. One may accordingly consider a simple “contact” (zero-range) potential $V_{\text{eff}}(\mathbf{r}) = v_0 \delta(\mathbf{r})$, where v_0 is a negative constant. A suitable regularization is required in this case to remove divergences that result in the diagrammatic structure. In three dimensions, it is common practice to introduce the fermionic *scattering length* a_F defined via (we set \hbar and Boltzmann’s constant equal to unity throughout)

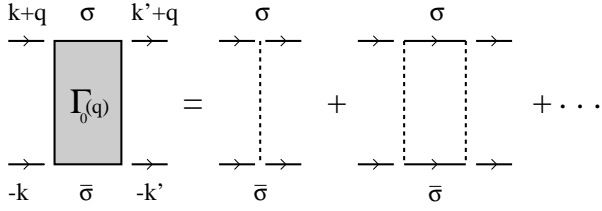
$$\frac{m}{4\pi a_F} = \frac{1}{v_0} + \int \frac{d\mathbf{k}}{(2\pi)^3} \frac{m}{\mathbf{k}^2}, \quad (2.1)$$

where \mathbf{k} is a wave vector and m the fermionic (effective) mass. The ultraviolet divergence on the right-hand side of Eq. (2.1) is compensated by letting $v_0 \rightarrow 0^-$ in a suitable way, as to keep a_F finite. This can be done, for instance, by introducing an ultraviolet cutoff k_0 and choosing v_0 such that¹⁴

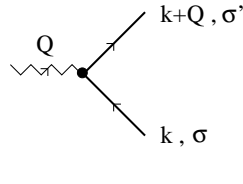
$$v_0 = -\frac{2\pi^2}{mk_0} - \frac{\pi^3}{ma_F k_0^2}, \quad (2.2)$$

with $k_0 \rightarrow \infty$ eventually. The evolution from the weak to strong coupling can now be tuned by varying the scattering length a_F , which is negative in the weak-coupling regime (where a bound-state has not yet appeared in the associated two-body problem) and positive in the strong-coupling (bosonic) regime (where a_F coincides with the bound-state radius).

The explicit form (2.2) for v_0 in terms of k_0 considerably simplifies the structure of the associated many-body perturbation theory, as discussed in Ref. 14. It was shown there that the effects of the interaction survive *only* in the particle-particle ladder depicted in Fig. 1(a), while connections among different ladders (as well as other links required to form, e.g., fermionic self-energies and correlation functions) are provided by the bare single-particle fermionic Green’s functions. In particular, a current (or density or spin) vertex represented in Fig. 1(b) is required to connect the external (electromagnetic) coupling with the structure of the fermionic two-particle Green’s function and obtain the response functions.



(a)



(b)

FIG. 1. (a) Particle-particle ladder, where full and broken lines represent fermionic bare single-particle Green's functions and interactions, respectively (four-momenta and spin labels are indicated); (b) Current (or density or spin) vertex connecting the external (electromagnetic) disturbance to the fermionic two-particle Green's function.

The general expression of the particle-particle ladder of Fig. 1(a) for any temperature and value of a_F reads:¹⁴

$$\Gamma_0(q) = - \left\{ \frac{m}{4\pi a_F} + \int \frac{d\mathbf{k}}{(2\pi)^3} \times \left[\frac{\tanh(\beta\xi(\mathbf{k})/2) + \tanh(\beta\xi(\mathbf{k}-\mathbf{q})/2)}{2(\xi(\mathbf{k}) + \xi(\mathbf{k}-\mathbf{q}) - i\omega_\nu)} - \frac{m}{\mathbf{k}^2} \right] \right\}^{-1} \quad (2.3)$$

with the four-vector notation $q \equiv (\mathbf{q}, \omega_\nu)$, where \mathbf{q} is a wave vector, $\omega_\nu = 2\nu\pi\beta^{-1}$ (ν integer) a bosonic Matsubara frequency, $\beta = 1/T$ the inverse temperature, and $\xi(\mathbf{k}) = \mathbf{k}^2/(2m) - \mu$ (μ being the fermionic chemical potential). This expression acquires a particularly simple form both in the strong- and weak-coupling limit.

In the strong-coupling limit, μ approaches the value $-\epsilon_0/2$ where $\epsilon_0 = (ma_F^2)^{-1}$ is the binding energy of the associated two-body problem. As ϵ_0 increases without bound in strong coupling, at any finite temperature we may consider the limit $\beta\mu \rightarrow -\infty$ in Eq. (2.3). One thus gets the *polar structure*:¹⁴

$$\Gamma_0(q) \cong - \frac{8\pi}{m^2 a_F} \frac{1}{i\omega_\nu - \frac{\mathbf{q}^2}{4m} + \mu_B} \quad (2.4)$$

where $\mu_B = 2\mu + \epsilon_0$. Apart from the residue being different from unity, this expression has the form of a free propagator for (composite) bosons with mass $m_B = 2m$ and chemical potential μ_B . It is important to emphasize that

Eq. (2.4) holds provided $|\omega_\nu| \ll \epsilon_0$ and $\mathbf{q}^2/(4m) \ll \epsilon_0$, which can in practice be satisfied for all relevant values of ω_ν and \mathbf{q} when ϵ_0 is sufficiently large.

In the weak-coupling limit, on the other hand, the chemical potential is (slightly) smaller than the Fermi energy $\epsilon_F = k_F^2/(2m)$ (k_F being the Fermi wave vector) for temperatures much smaller than ϵ_F itself. In this case, the particle-particle ladder (2.3) acquires the form characteristic of superconducting fluctuation theory:³

$$\Gamma_0(q) \cong \frac{1}{N_0} \frac{1}{\frac{T-T_c}{T_c} + \eta\mathbf{q}^2 + \gamma|\omega_\nu|} \quad (2.5)$$

where N_0 is the free-fermion density of states at the Fermi level (per spin component), $(T - T_c) \ll T_c$ where T_c is the BCS critical temperature, $\gamma = \pi/(8T_c)$, and

$$\eta = \frac{7\zeta(3)}{48\pi^2} \left(\frac{k_F}{mT_c} \right)^2 \quad (2.6)$$

in three dimensions ($\zeta(3) \approx 1.202$ being the Riemann zeta function of argument 3).

In the strong-coupling limit, one expects on physical grounds the response functions of the original Fermi system to be expressed only in terms of composite-boson structures, namely, bosonic propagators and vertices. As anticipated in the Introduction, the evolution of the response functions from strong to weak coupling rests on the particle-particle ladder (which in the strong-coupling limit has the form of a composite-boson propagator [cf. Eq. (2.4)]) becoming the building block of fluctuation theory in the weak-coupling limit *above* the superconducting critical temperature [cf. Eq. (2.5)].

We pass now to identify the relevant bosonic diagrams for the current response function and map them onto the corresponding fermionic diagrams.

A. Leading diagrams

For a system of noninteracting bosons, the current response function is depicted diagrammatically in Fig. 2(a). This diagram represents the leading contribution to the current response function also for a system of bosons at sufficiently *low density* and interacting via a (repulsive) finite-range potential.

Mapping of this (as well as other) bosonic diagram(s) onto a corresponding set of fermionic diagrams can be obtained according to the following *prescriptions*: (i) Remove from the bosonic diagram the two outer vertices representing the bosonic coupling to the external field and get a bosonic diagram “open” at its ends; (ii) Replace the bare bosonic propagators by the composite boson propagators given by Eq. (2.4); (iii) Connect the ensuing (fermionic) diagram to the fermionic vertex of Fig. 1(b) representing the fermionic coupling to the external field; (iv) Contract eventually the remaining dangling

ends of the particle-particle ladders among themselves in accordance with their spin structure.

In this way, besides those fermionic diagrams which correctly reproduce the value of the original bosonic diagram in the strong-coupling limit, additional fermionic diagrams may result which do not have a bosonic analogue in the strong-coupling limit and whose value is therefore considerably suppressed in this limit. These additional diagrams will consistently be dismissed when establishing a mapping between the original bosonic diagrams and the associated fermionic diagrams.

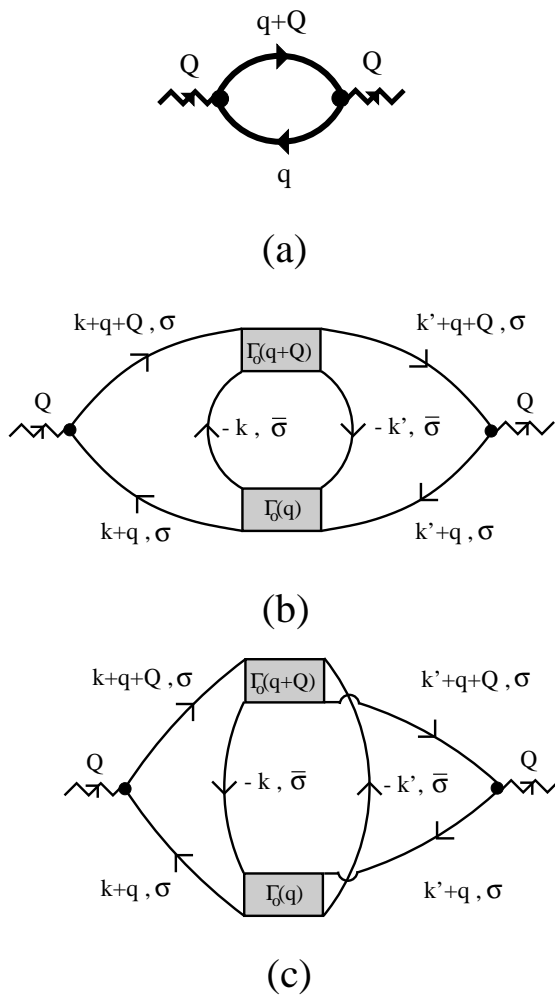


FIG. 2. (a) Current response function for an ideal Bose gas above the Bose-Einstein temperature, where thick lines represent bosonic bare single-particle Green's functions; (b)-(c) Corresponding current response function for a system of composite bosons.

With these prescriptions, the fermionic diagrams of Figs. 2(b) and 2(c) are generated from the bosonic diagram of Fig. 2(a), with a degeneracy factor of 2 each due to the fermionic spin multiplicity. (An additional diagram, which corresponds to a self-energy decoration of both bare fermionic propagators of the fermionic particle-hole bubble, is also generated according to the above pre-

scriptions. Since this diagram does not have a bosonic analogue in the strong-coupling limit, it will not be considered in the following according to the above discussion.) Although the two diagrams 2(b) and 2(c) are topologically not equivalent, their expressions coincide for particle-particle ladders corresponding to a point-contact potential. We may thus consider only one of these diagrams (say, diagram 2(b)) with a multiplicity factor of 4.

This diagram contains two (vector) factors of the type:

$$\mathbf{J}(q, Q) = \frac{1}{\beta} \sum_{\omega_n} \int \frac{d\mathbf{k}}{(2\pi)^3} \frac{[2(\mathbf{k} + \mathbf{q}) + \mathbf{Q}]}{2m} \times \mathcal{G}^0(-k) \mathcal{G}^0(k + q) \mathcal{G}^0(k + q + Q) \quad (2.7)$$

where $Q \equiv (\mathbf{Q}, \Omega_\nu)$ and $k \equiv (\mathbf{k}, \omega_n)$ are bosonic and fermionic four-vectors, respectively, and $\mathcal{G}^0(k) = (i\omega_n - \xi(\mathbf{k}))^{-1}$ is a fermionic bare propagator ($\omega_n = (2n + 1)\pi\beta^{-1}$ (n integer) being a fermionic Matsubara frequency). Symmetry arguments show that $\mathbf{J}(q, Q)$ is directed along $(2\mathbf{q} + \mathbf{Q})$, allowing us to set

$$\mathbf{J}(q, Q) = \frac{(2\mathbf{q} + \mathbf{Q})}{2m} C(q, Q). \quad (2.8)$$

The (scalar) factor $C(q, Q)$ can be readily evaluated in the strong-coupling limit for vanishing external four-vector ($Q = 0$). In this limit, the Fermi functions originating from the sum over ω_n in Eq. (2.7) vanish exponentially like $\exp(-\beta|\mu|)$, yielding

$$C(q, Q = 0) \approx -\frac{m^{3/2}}{16\pi} \frac{1}{\sqrt{2|\mu|}} \quad (2.9)$$

at the leading order in $|\omega_\nu/\mu|$ and $\mathbf{q}^2/(2m|\mu|)$. With these approximations, the value of the diagram of Fig. 2(b) for $Q = 0$ becomes (the “static” limit with $\Omega_\nu = 0$ and $\mathbf{Q} \rightarrow 0$ is actually implied):

$$\chi_j(Q = 0) \cong -4 \frac{1}{m^2} \frac{m^3}{(16\pi)^2} \frac{1}{2|\mu|} \left(\frac{8\pi}{m^2 a_F} \right)^2 \times \frac{1}{\beta} \sum_{\omega_\nu} \int \frac{d\mathbf{q}}{(2\pi)^3} \frac{\mathbf{q} \cdot \mathbf{q}}{\left(i\omega_\nu - \frac{\mathbf{q}^2}{4m} + \mu_B \right)^2} \quad (2.10)$$

where the overall minus sign complies with the definition of the current response function χ_j , the factor of 4 represents the degeneracy of the diagram, and the remaining factors stem from Eqs. (2.9) and (2.4), in the order. Apart from the degeneracy factor of 4, expression (2.10) coincides with the $Q = 0$ limit of the current response function for a system of (composite) bosons with mass $m_B = 2m$ and chemical potential μ_B , when for $|\mu|$ one uses the expression $(2ma_F^2)^{-1}$ which holds in the strong-coupling limit. Each diagonal component of this bosonic current tensor then equals $-n_B/m_B$, where the bosonic density $n_B = n/2$ is half the original fermionic density n .

The degeneracy factor of 4 in Eq. (2.10) restores eventually the correct value $-n/m$ for the diagonal component of the fermionic current response function, in accordance with the f-sum rule.¹⁸

It is further evident that, when using for the particle-particle ladders in diagram 2(b) the expression (2.5) valid in the weak-coupling limit close to T_c , one recovers the Aslamazov-Larkin contribution to the current response function,³ which represents the leading fluctuation contribution to this response function in the weak-coupling limit.

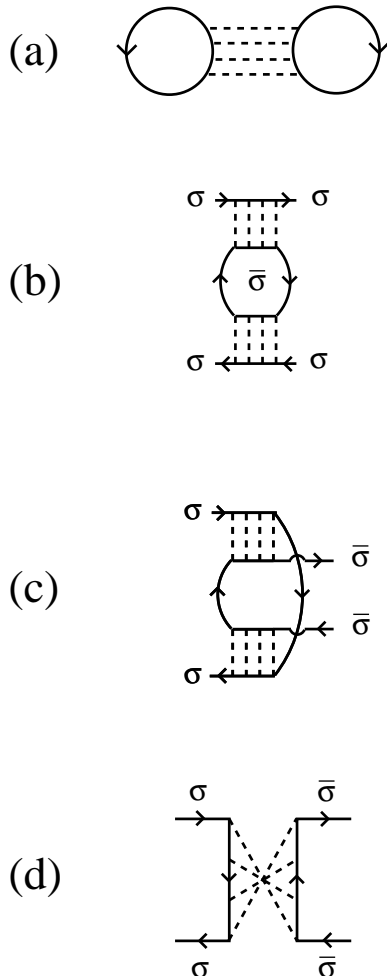


FIG. 3. (a) “Potential” from which the diagrams of Figs. 2(b) and 2(c) are generated by the Baym’s prescriptions; (b)-(d) Fermionic effective two-particle interaction derived from the “potential” (a) (with spin labels corresponding to a contact interaction).

A possible scheme to interpolate between weak and strong coupling for the current response function (and thus to address the interesting intermediate-coupling regime) may thus be to consider the diagram of Fig. 2(b) together with the fermionic bare particle-hole bubble. In this way, in the weak-coupling limit one retains the free-fermion result plus its AL fluctuation correction while in

the strong-coupling limit one recovers the free-boson result, which represent the dominant contributions in the respective limits. For addressing specific issues, however, it might be relevant to include also additional diagrams which contribute to the weak-to-intermediate coupling regime but are suppressed in the strong-coupling limit.

It is interesting to mention that the AL diagrams of Figs. 2(b) and 2(c) for the response function can be obtained directly in fermionic language via Baym’s prescriptions,¹⁹ using the “potential” depicted in Fig. 3(a). Taking two successive functional derivatives with respect to the fermionic single-particle propagators (which, in this case, are meant to be self-consistent) yields, in fact, the fermionic effective two-particle interaction depicted in Figs. 3(b)-(d), which acts as the kernel of the Bethe-Salpeter equation for the two-particle Green’s function. It is then clear that diagrams 2(b) and 2(c) result, respectively, by connecting diagrams 3(b) and 3(c) with the fermionic vertex of Fig. 1(b), while connecting diagram 2(d) with the fermionic vertex of Fig. 1(b) yields the Maki-Thompson diagram,⁴ to be discussed in Section II.C.

B. Next-to-leading diagrams

We pass now to examine higher-order diagrams in the bosonic *diluteness parameter* $n_B^{1/3}a_B$, where a_B is the scattering length associated with the residual interaction between composite bosons.²⁰

The bosonic diagram, which is next-to-leading with respect to the diagram of Fig. 2(a), is depicted in Fig. 4(a), where the dark square in the middle represents a (symmetrized) bosonic interaction.¹⁷ It is, in fact, the presence of an *additional* bosonic *cycle* in diagram 4(a) with respect to diagram 2(a) which accounts for an additional power in the bosonic density in the expression of this diagram. (A further bosonic diagram of the same order in the density can be obtained from the diagram of Fig. 2(a), by dressing one of the two bosonic propagators with a low-density self-energy, as in the theory of an interacting “dilute” Bose system.¹⁷)

The bosonic diagram of Fig. 4(a) can be mapped into a corresponding set of diagrams for the fermionic response function(s), according to the rules developed in Ref. 14 and to the prescriptions stated in Section II.A. In this way, one ends up with the two fermionic diagrams reported in Figs. 4(b) and 4(c), with a degeneracy factor of 8 and 4, in the order, after having taken into account that expressions of topologically not equivalent diagrams may coincide for a fermionic point-contact potential. While the diagram of Fig. 4(b) has a meaningful strong-coupling limit in terms of composite-boson propagators, the diagram of Fig. 4(c) lacks a bosonic representation and yields consistently a subleading contribution in this limit. For these reasons, one may retain diagram 4(b) and disregard diagram 4(c) to follow the evolution from weak to

strong coupling.

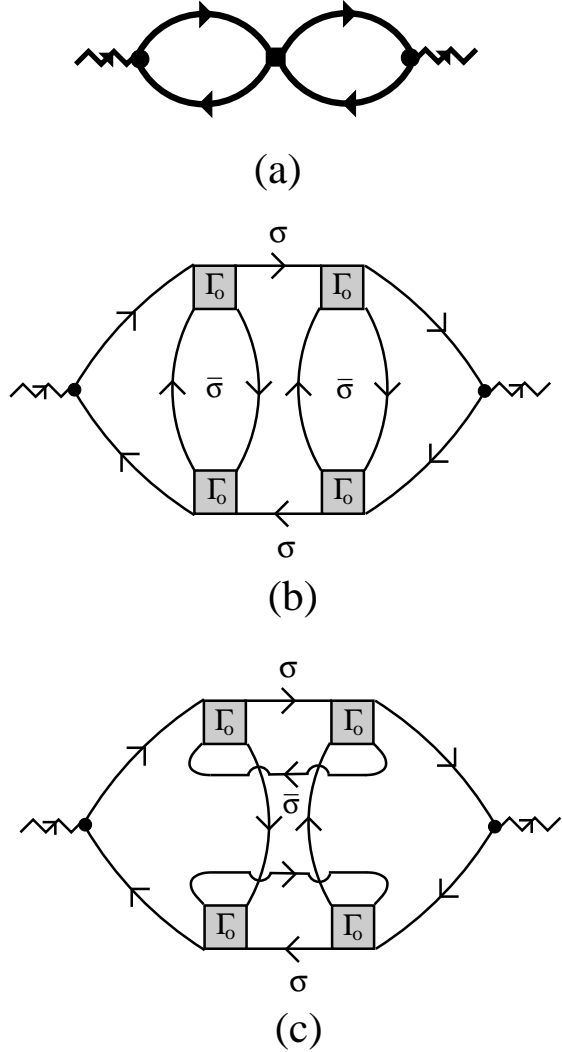


FIG. 4. (a) Next-to-leading bosonic diagram in the “dilute” limit; (b) Fermionic diagram corresponding to the bosonic diagram (a); (c) Subleading diagram generated from diagram (a).

To verify that to diagram 4(b) there corresponds a meaningful strong-coupling limit, we evaluate the central part of this diagram for $Q = 0$ and obtain:

$$\begin{aligned} & \frac{1}{\beta} \sum_{\omega_{n''}} \int \frac{d\mathbf{k}''}{(2\pi)^3} \mathcal{G}^0(-\mathbf{k}'') \mathcal{G}^0(\mathbf{k}'' + \mathbf{q}') \\ & \times \mathcal{G}^0(-\mathbf{k}'' + \mathbf{q} - \mathbf{q}') \mathcal{G}^0(\mathbf{k}'' + \mathbf{q}') \approx \frac{(ma_F)^3}{16\pi} \end{aligned} \quad (2.11)$$

where use has been made of the relation $2|\mu| \approx \epsilon_0 = (ma_F^2)^{-1}$ that holds in this limit. The diagram 4(b) thus contains the factors

$$-\left(-\frac{m^2 a_F}{8\pi}\right)^2 \left(-\frac{8\pi}{m^2 a_F}\right)^4 \frac{(ma_F)^3}{16\pi} = -\frac{4\pi a_F}{m} \quad (2.12)$$

which arise, respectively, from the current vertex (cf. Eq. (2.9)), from the residue of the particle-particle ladder (cf. Eq. (2.4)), and from the central part (2.11), while the overall minus sign is due to the presence of three fermionic loops. In this way, the strength $v(0) = 4\pi a_F/m$ of the residual interaction between composite bosons discussed in Ref. 11 has been correctly reconstructed, and the diagram of Fig. 4(b) gives a faithful representation of the bosonic diagram of Fig. 4(a).

It is again interesting to mention that diagram 4(b) (with a degeneracy factor of 8) can be obtained directly in fermionic language by: Considering the fermionic effective two-particle interaction depicted in Figs. 3(b) and 3(c) to appear *twice* in the two-fermion Green’s function; Connecting the ensuing four diagrams with the fermionic vertex of Fig. 1(b); Recognizing the equivalence of these four diagrams; Summing eventually over the spin components. One may, in fact, say that the diagram of Fig. 4(c) is *not reducible* in the (fermionic) two-particle channel and corresponds to a choice of the fermionic effective two-particle interaction different from 3(b) and 3(c).

Finally, one can estimate that the ratio of diagram 4(c) to diagram 4(b) is of the order

$$\frac{m}{a_F} \frac{(na_F^3)^2}{\frac{\partial n}{\partial \mu}}, \quad (2.13)$$

which is indeed much smaller than unity in the low-density limit ($n_B^{1/3} a_B \ll 1$) provided the compressibility $(\partial n / \partial \mu)$ does not vanish.²¹

III. SUBLEADING DIAGRAMS

We consider next additional diagrams (besides diagram 4(c) already considered in Section II.B) which are subleading in the strong-coupling limit, such as the Mak-Thompson response diagram, that is obtained by connecting the effective two-particle interaction of Fig. 3(d) with the external coupling of Fig. 1(b). This diagram has been extensively studied in the weak-coupling limit in the context of the theory of superconducting fluctuations.^{4–6} As this diagram contains *only one* particle-particle ladder, one expects it to have no analogue in bosonic language (at least for the normal phase) and consequently not to contribute to the response functions in the strong-coupling limit. Upon evaluating this diagram for the current response function in the strong-coupling limit at $Q = 0$, however, one obtains the finite value n/m (including spin multiplicity).

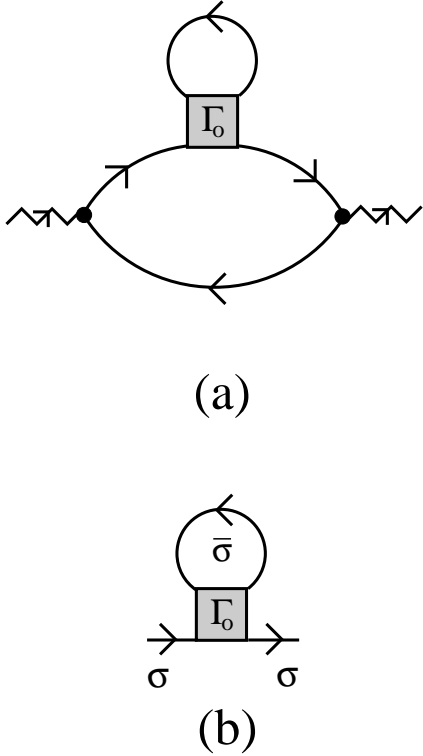


FIG. 5. (a) DOS diagram for the response functions; (b) Self-energy diagram for a “dilute” Fermi gas.

This contradiction can be overcome by considering at the same time the density-of-state (DOS) diagram depicted in Fig. 5(a) (with a multiplicity factor of 4), obtained by making the fermionic self-energy insertion of Fig. 5(b) into the fermionic particle-hole bare bubble. In the strong-coupling limit, diagram 5(a) gives, in fact, the contribution $-n/m$ to the $Q = 0$ current response function, thus cancelling exactly the contribution of the MT diagram.^{22,23}

This example shows that the diagrams for the response functions need to be grouped into suitable sets, in order to get a meaningful strong-coupling limit. The grouping procedure appears to be especially relevant for the spin response function, that ought to vanish in the strong-coupling limit for (composite) spin-zero bosons, as discussed in the next Section.

IV. DENSITY AND SPIN RESPONSE FUNCTIONS

In this Section, we complement the analysis of the strong-coupling limit by analyzing the density and spin response functions associated with the AL, MT, and DOS diagrams (which are usually considered in the weak-coupling limit for the theory of superconducting fluctuations^{5,6}). In addition, we discuss the set of diagrams that needs to be associated with a given sub-leading diagram (for instance, the diagram of Fig. 4(c))

for the spin response function to be *exponentially* suppressed in the strong-coupling limit, as required on physical grounds.

The contribution to the density response function from the AL diagram contains two (scalar) factors of the type

$$D(q, Q) = \frac{1}{\beta} \sum_{\omega_n} \int \frac{d\mathbf{k}}{(2\pi)^3} \mathcal{G}^0(-k) \mathcal{G}^0(k+q) \times \mathcal{G}^0(k+q+Q), \quad (4.1)$$

which can be readily evaluated in the strong-coupling limit for $Q = 0$, to give

$$D(q, Q = 0) \approx -\frac{m^2 a_F}{8\pi}. \quad (4.2)$$

This factor thus cancels the residue of the particle-particle ladder (2.4) in the strong-coupling limit, yielding for the density response function the expression valid for the ideal Bose gas:

$$\chi_n(Q) \cong -4 \frac{1}{\beta} \sum_{\omega_\nu} \int \frac{d\mathbf{q}}{(2\pi)^3} \frac{1}{i\omega_\nu - \frac{\mathbf{q}^2}{4m} + \mu_B} \times \frac{1}{i\omega_\nu + i\Omega_\nu - \frac{(\mathbf{q}+\mathbf{Q})^2}{4m} + \mu_B}. \quad (4.3)$$

Here, the minus sign is due to the definition of the density response function and the factor of 4 accounts for the degeneracy of the diagram. In the “static” ($\Omega_\nu = 0$ and $\mathbf{Q} \rightarrow 0$) and “dynamic” ($\mathbf{Q} = 0$ and $\Omega_\nu \rightarrow 0$) limits this expression correctly recovers the values $-4\partial n_B/\partial \mu_B = -\partial n/\partial \mu$ and 0, in the order.

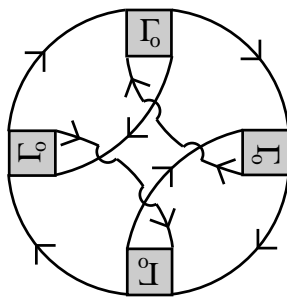
Concerning the spin correlation function, the contributions to χ_{zz} from the AL diagrams of Fig. 2(b) and 2(c) cancel each other *identically* for all coupling strengths (these diagrams, on the other hand, do not contribute to χ_{xx} and χ_{yy} owing to their spin structure). This result is consistent with the expectation that in the strong-coupling limit the AL diagrams provide a faithful representation for the (spinless) ideal Bose gas.

Contrary to the case of the current response function treated in Section II.C, in the strong-coupling limit the contributions to the ($Q = 0$) density response function from the MT diagram of Fig. 3(d) and the DOS diagram of Fig. 5(a) do not cancel each other. Rather, each of them equals $-ma_F^2 n_B = -n/(4|\mu|)$, which however vanishes as $|\mu|$ increases in the strong-coupling limit.

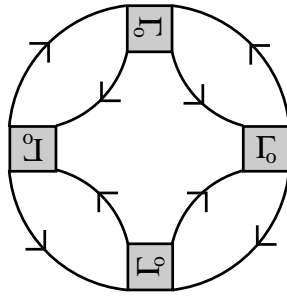
The contributions to the spin correlation function χ_{zz} from the MT and DOS diagrams cancel instead each other for $Q = 0$ in the strong-coupling limit, since the MT contribution acquires an extra minus sign with respect to the DOS contribution. This implies that the spin response function obtained by considering these two diagrams simultaneously vanishes *exponentially* like $\exp(-\beta|\mu|)$ in the strong-coupling limit, due to the behavior of the Fermi functions in this limit. This is precisely what one would expect on physical grounds,

since a non-vanishing spin response for spin-zero composite bosons should only result when the temperature is comparable with their binding energy and the composite bosons break apart. In this context, it is interesting to mention that the progressive vanishing of the spin susceptibility upon approaching the strong-coupling limit has been confirmed by Monte Carlo results for the negative- U Hubbard model,²⁴ (even though it is not easy to extract the predicted exponential behavior from the limited set of Monte Carlo data).

The vanishing of the spin response function in the strong-coupling limit could, in fact, be taken as a *physically meaningful criterion* for grouping sets of diagrams in an appropriate way (diagrams which may as well be considered for the calculation of the current and density response functions).



(a)



(b)

FIG. 6. (a)-(b) Diagrams for the thermodynamic potential, from which the contributions of Figs. 4(b) and 4(c) to the static spin susceptibilities can be derived.

For instance, while the diagram of Fig. 4(b) leads to a meaningful strong-coupling limit (with the associated spin response function vanishing *identically* by the same reasons mentioned above for the AL diagram(s)), the diagram of Fig. 4(c) (which was regarded in Section II.B to be subleading as far as the current response was con-

cerned) yields a contribution to the spin response function which is not *exponentially* vanishing, as it would be required in the strong-coupling limit. Additional diagrams have then to be associated with the diagram of Fig. 4(c) to obtain the correct exponential behavior for the spin response function.

To this end, we consider the two contributions to the thermodynamic potential depicted schematically in Figs. 6(a) and 6(b) and perform all possible ($Q = 0$) magnetic-field insertions in the fermionic single-particle propagators, as to get the “static” spin susceptibility (by this procedure, no additional contributions are obtained by making magnetic-field insertions inside the particle-particle ladder in the strong-coupling limit). In this way, two sets of six diagrams each result, which include, by construction, the diagram of Fig. 4(c) (counted twice, due to the equivalence of two diagrams for the case of a point-contact potential) plus decorations of the AL, MT, and DOS diagrams. In the strong-coupling limit (when all terms proportional to the Fermi functions are exponentially suppressed), it can then be shown that the contributions to the spin response function χ_{zz} from the six diagrams obtained from Fig. 6(a) (as well from the six diagrams obtained from Fig. 6(b)) add up to zero.

To summarize, we have argued that for diagrams representing the response functions (constructed in terms of the original fermionic single-particle interaction and propagators) to have a meaningful strong-coupling limit (as far as the current and density response is concerned) in terms of the residual bosonic interaction and composite-boson propagators, their contributions to the spin response function should vanish *identically*. For other diagrams that do not have a meaningful strong-coupling limit, on the other hand, their contributions to the spin response function in the strong-coupling limit will instead vanish exponentially like $\exp(-\beta|\mu|)$, provided these diagrams are grouped into suitable sets as shown explicitly by the examples considered above. No definite criterion for selecting the dominant diagrammatic contributions to the *spin* correlation function starting from the strong-coupling limit can thus be formulated. The only care one should exert in this case is to suitably group a given selected diagram with its companions, as to get an exponentially vanishing spin response function in the strong-coupling limit.

V. CONCLUDING REMARKS

In this paper, we have examined the evolution from the weak to strong coupling of the response functions for a three dimensional (clean) Fermi system with an attractive interaction above its critical temperature. While in the weak-coupling limit the standard analysis of superconducting fluctuations applies, we have shown that in the strong-coupling limit the original fermionic response functions map *directly* into the response functions of a

system of composite bosons.

We have shown that only those fermionic diagrams, to which there corresponds a meaningful representation in terms of composite bosons, contribute to the strong-coupling limit. The AL, MT, and DOS diagrams of superconducting-fluctuation theory have been analyzed among others. We have further argued that the analysis of the spin response function may also serve to identify diagrams which survive in the strong-coupling limit.

It is evident that the diagrammatic contributions to the response functions are much more numerous in the weak- than in the strong-coupling limit, since many diagrams contributing to the weak-coupling limit are suppressed in the strong-coupling limit. If the relevant diagrams for the response functions were only selected starting from the strong-coupling limit, one might then evidently run the risk of missing non-vanishing and possibly important contributions when extrapolating these diagrams to the weak-coupling limit. This is especially true for the spin response function, which vanishes for a system of spinless bosons: extrapolating to the weak-coupling limit diagrams that contribute in the bosonic limit to the current and density response functions, would then result into a vanishing spin response function for *all* coupling strengths. It is for these reasons that the finding of the AL diagram representing the dominant contribution to the momentum and frequency dependent current and density response functions (over and above the free-fermion contribution), *both* in weak coupling (where it is associated with superconducting fluctuations near the critical temperature) and in strong coupling (for a “dilute” system of composite bosons), should be regarded as a nontrivial result of the present analysis.

Controlling the two (weak- and strong-coupling) limits by a *single theory* may prove especially important when one is interested in the intermediate (crossover) region (as it might be the case for high-temperature superconductors). One reasonable strategy to approach the crossover region appears thus to *interpolate* between theories that can be controlled in the two (weak- and strong-coupling) limits. This could be done, for instance by including all diagrams which are dominant either in the weak- or in the strong-coupling limit (according to the respective relevance criteria) and evaluating them in all coupling regimes.

Finally, it is interesting to comment on the recent results reported in Ref. 25 regarding the temperature dependence of the density and spin susceptibilities for a two-dimensional negative- U Hubbard model, calculated, respectively, via the AL and MT diagrams and compared with available Monte Carlo results for $U = -4t$ (t being the nearest-neighbor hopping). These authors find a remarkable agreement between their calculation and the Monte Carlo data for the spin susceptibility, provided the mass term in the particle-particle ladder (2.5) is replaced by a mass term with the temperature dependence characteristic of the Kosterlitz-Thouless theory. For the density susceptibility, however, this replacement alone is

not enough to reproduce the Monte Carlo data. The discussion presented in Section II.B, in fact, suggests that modifications of the AL diagram(s) obtained by considering bosonic self-energy corrections to the particle-particle ladder should be accompanied by the inclusion of additional diagrams, which account for the residual bosonic interaction at the *same* order in the diluteness parameter in the strong-coupling limit.

In this paper, we have considered the response functions in the normal phase *above* the critical temperature. It would certainly be interesting to extend this analysis *below* the superconducting critical temperature and study the continuous evolution of the response functions from the weak-coupling limit of (BCS) superconductivity to the strong-coupling limit where Bose-Einstein condensation takes place. In this case, one would expect a description in terms of Bogoliubov quasi-particles to be appropriate for a “dilute” system of composite bosons (at least close to zero temperature), with the superfluid density being affected at finite temperature by sound modes in the strong-coupling limit and by pair-breaking effects in the weak-coupling limit. Which of these two effects dominate in the intermediate (crossover) region is a challenging question, which can be addressed only by numerical calculations of a suitable set of diagrams. Work along these lines is in progress.

ACKNOWLEDGMENTS

The authors are indebted to C. Castellani, A. Perali, and A. Varlamov for helpful discussions. Partial financial support from the Italian INFM under Contract PAIS Crossover No. 269 is gratefully acknowledged.

¹ J.R. Schrieffer, *Theory of Superconductivity* (Benjamin, New York, 1964).

² See, e.g., A.L. Fetter and J.D. Walecka, *Quantum Theory of Many-Particle Systems* (McGraw-Hill, New York, 1971), Chapter 13.

³ L.G. Aslamazov and A.I. Larkin, Sov. Phys. JETP **10**, 875 (1968).

⁴ R.S. Thompson, Phys. Rev. B **1**, 327 (1970); J.P. Hurault and K. Maki, Phys. Rev. B **2**, 2560 (1970).

⁵ W. J. Skocpol and M. Tinkham, Rep. Prog. Phys. **38**, 1049 (1975).

⁶ A.A. Varlamov, G. Balestrino, E. Milani, and D.V. Livanov, Adv. Phys. **48**, 655 (1999).

⁷ H. Ding *et al.*, Nature **382**, 51 (1996); and Phys. Rev. Lett. **78**, 2628 (1997).

⁸ A. G. Loeser *et al.*, Science **273**, 325 (1996).

⁹ C.A.R. Sá de Melo, M. Randeria, and J.R. Engelbrecht, Phys. Rev. Lett. **71**, 3202 (1993).

- ¹⁰ R. Haussmann, Z. Phys. B **91**, 291 (1993).
- ¹¹ F. Pistolesi and G.C. Strinati, Phys. Rev. B **49**, 6356 (1994); *ibid.* B **53**, 15168 (1996).
- ¹² S. Stintzing and W. Zwerger, Phys. Rev. B **56**, 9004 (1997).
- ¹³ B. Jankó, J. Maly, and K. Levin, Phys. Rev. B **56**, R11407 (1997).
- ¹⁴ P. Pieri and G.C. Strinati, Phys. Rev. B **61**, 15370 (2000), and cond-mat/9811166.
- ¹⁵ A.J. Leggett, in *Modern Trends in the Theory of Condensed Matter*, edited by A. Pekalski and R. Przystawa, Lecture Notes in Physics Vol.115 (Springer-Verlag, Berlin, 1980), p.13.
- ¹⁶ P. Nozières and S. Schmitt-Rink, J. Low. Temp. Phys. **59**, 195 (1985).
- ¹⁷ V.N. Popov, *Functional Integrals and Collective Excitations* (Cambridge University Press, Cambridge, 1987).
- ¹⁸ G. Baym, in *Mathematical Methods in Solid State and Superfluid Theory*, R.C. Clark and G.H. Derrick, Eds. (Oliver and Boyd, Edinburgh, 1967).
- ¹⁹ G. Baym, Phys. Rev. **127**, 1391 (1962).
- ²⁰ It was shown in Ref. 14 that the scattering length a_B for composite bosons is proportional to the fermionic scattering length a_F , with a coefficient of order unity.
- ²¹ In the strong-coupling (bosonic) limit, one may write $\partial n / \partial \mu = 4 \partial n_B / \partial \mu_B$ and estimate $\partial n_B / \partial \mu_B$ from the relation $\mu_B(n_B)$ valid for an ideal Bose gas close to the Bose-Einstein temperature T_{BE} (cf. Ref. 2, Section 5). One obtains $\partial \mu_B / \partial n_B \approx 1.63(T - T_{BE})/n_B$, yielding a divergent $\partial n_B / \partial \mu_B$ as T approaches T_{BE} , which further suppresses diagram 4(c) with respect to diagram 4(b).
- ²² In the strong-coupling (bosonic) limit, the Q dependence of the MT and DOS diagrams are expected to be irrelevant insofar as the fermionic chemical potential constitutes the largest energy scale in the problem.
- ²³ A similar cancellation has been noted in the weak-coupling limit by D.V. Livanov, G. Savona, and A.A. Varlamov, Phys. Rev. B (in press).
- ²⁴ M. Randeria, N. Trivedi, A. Moreo, and R.T. Scalettar, Phys. Rev. Lett. **69**, 2001 (1992); J.M. Singer *et al.*, Phys. Rev. B **54**, 1286 (1996).
- ²⁵ L. Benfatto, A. Perali, C. Castellani, and M. Grilli, Eur. Phys. J. B **13**, 609 (2000).